FLUID WRAP AROUND DURING WET CHEMICAL SINGLE SIDE TREATMENTS

M.Richter(1), S. Narayanan(1), A. Hain(2), M. Zimmer(1), J. Rentsch(1), H. Reinecke(3)
(1)Fraunhofer-Institute for Solar Energy Systems (ISE), Heidenhofstr 2, D-79110 Freiburg, Germany, +49 761 4588-5654
(2)SINGULUS TECHNOLOGIES AG, Hanauer Landstr. 103, 63796 Kahl am Main, Germany
(3)Department of Microsystems Engineering, IMTEK, University Freiburg, Georges-Köhler-Allee-103, 79110, Freiburg, Germany

ABSTRACT: Single sided etching is commonly used for processing solar cells. As with all single sided processes using wet etching solutions, fluid wrap around appears. This paper investigates this effect in two ways. Different experimental setups will be shown and described including results and theories concerning the fluid wrap around. It can be proven, that bursting bubbles caused by etching support the fluid wrap around as well as some additives and surface morphologies. Additionally, surface tension, surface energy and surface morphologies can be found as influencing factors. Further investigations for better understanding of the fluid wrap around will be described.
Keywords: single side wet etching, polishing, fluid wrap around

1 INTRODUCTION

For high efficiency solar cell concepts there is a need for separate treatments to the front and rear side of a silicon wafer [1]. A smooth polished rear surface is desirable for passivated cell concepts (e.g. PERC) as the flat surface decreases the surface recombination velocity and leads to an increase in light trapping [2]. In current state of the art, cells are texturized on both sides resulting in a rather rough surface which is disadvantageous for the rear side [3]. Therefore an inline single-sided polishing step is introduced directly after texturization. Following this, the emitter is constructed using a double-sided diffusion process. To avoid a short circuit between the front and the rear side of the solar cell, the emitter on the rear side is removed in a further wet chemical process step. Thereby resulting in two single-sided wet chemical processes, one before and one after the diffusion process. In terms of cost reduction there is the intention to merge both processes into one step [4] (Figure 1).

Figure 1: Process scheme for the PERC solar cell concept with the standard process (left) and combined wet chemical process (right). The orange highlighted steps are two side processes and the purple highlighted are single sided process steps.

The simplified sequence produces a solar cell process with one process step less in comparison to the standard process.

The current state of the art for single side etching is based on rollers (Figure 2) or a chain-system (Figure 3). For both principles the etching solution contacts the wafer from the bottom via the rollers or a high etch solution level (Figures 2-4). Thus a meniscus develops at the lower edge of the wafer and etching solution.

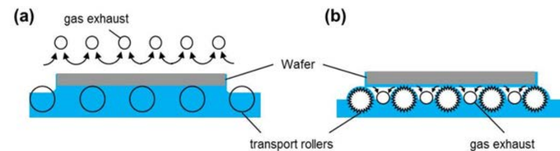

Figure 2: Transport by rollers. In (a) the contact between wafer and etch mixture happens via a meniscus because of a high bath level. An exhaust is at the borders of the transport line above the wafer level. In (b) the liquid is transported to the wafer surface by grooves in the rollers. The gas exhaust is between the rollers [2].

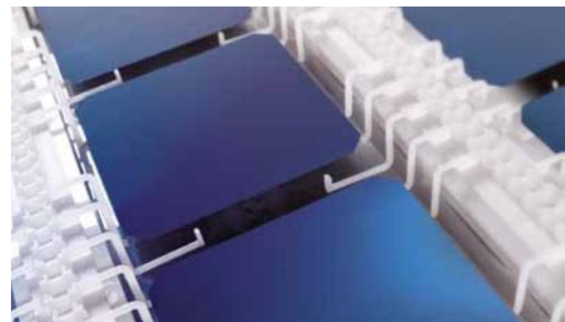

Figure 3: Transport by chain on pins. The wafer lies on 8 pins going through the etching mixture. There is no contact between the mechanical parts and the etch mixture or the wafer besides these eight small legs.

Due to meniscus the etching solution is able to wrap around onto the front side. This effect is observed with greater or lesser strength for all wet chemical single side processes.

In this paper the process of investigating the fluid wrap around is presented. Improvements of a theory explaining the basic mechanisms of the fluid wrap around will be shown.

2 FLUID WRAP AROUND

There are different factors influencing the front and rear surface of single side etched wafers (Figure 4).
The front side has to be protected from two main sources of emitter damage. One is the fluid that wraps around onto

the front side destroying the local emitter and the surface texture. The other issue is the emitter damage due to waste gases reacting with the whole front side. The wraparound and the reactive gases can be controlled by modifying the etching mixture and the amount of material removed from the rear side. [5]

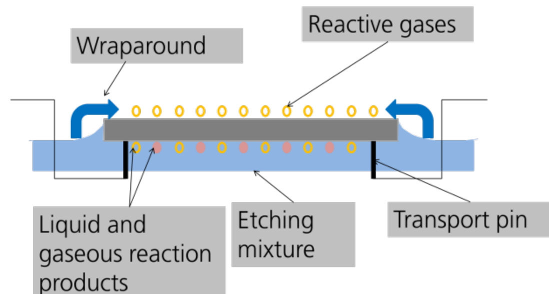

Figure 4: On the front and rear side different factors are affecting the etching result. On the front side the emitter and texturized surface has to be protected and on the rear side there can be inhomogeneous etching due to shadowing of the reactions products and transport system or an inappropriate etching mixture.

First theoretical considerations identified factors influencing the fluid wrap around. These are the surface energy of the sample, surface tension of the fluid, morphology of the surface, hydrophilic properties of the surface. Hydrophilic properties were supposed to have the most influence and have been investigated first.

While researching the wrap around it was observed that independent of the surface, whether hydrophilic or hydrophobic, the meniscus contacts the lower edge of the wafer, when contacting with an aqueous solution (figure 5) [5].

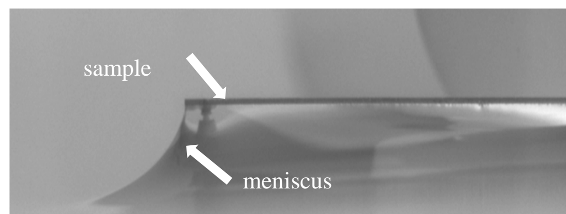

Figure 5: Hydrophilic wafer contacting with water. The meniscus contacts the wafer on the lower edge of the wafer [5].

Contacting the samples with HF-HNO_3 etching solution a reaction is induced. At the moment the reaction starts, gas bubbles rise and burst when they come out under the wafer. The bursting bubbles splash the wafer edge with etching solution and increase the meniscus. Furthermore, as the meniscus rises, the bursting bubbles splash even higher causing the meniscus to rise all the way up the edge on the front side of the wafer. [5].

Based on the observed interaction between fluid solution and wafer, first assumptions relating to experimental considerations were established. These are:

A) Fluid wrap around occurs due to splashing bubbles only

B) Hydrophilic and hydrophobic samples do not differ in behaviour concerning fluid wrap around and thus hydrophilic properties cannot have the highest influence on the wrap around.

In this experiment hydrophilic properties have been studied only. In order to prove these results and investigate more factors, new set ups and experiments were made. These will be shown during the further procedure.

3 EXPERIMENTAL

3.1 Sample preparation and characterization

Two sets of samples were prepared; figure 6 shows the process flow of both sample sets. Set A consists of 2 material types. Pseudo-square CZ-Si wafers 156 x 156 mm² in size were textured with an alkaline process and full-square mc-Si samples 156 x 156 mm² in size were textured with an acidic process. Half the samples of each material group were diffused on both sides in a $POCl_3$ process. In this set the morphology of the sample surface was varied by different texturing processes. Additionally the hydrophilic properties are varied within the groups with or without emitter diffusion and thus PSG.

Set B consists of alkaline textured pseudo-square CZ-Si wafers 156 x 156 mm² in size and acidic textured full-square mc-Si samples 156 x 156 mm² in size. These samples were symmetrically polished on both sides. The amount of silicon removal while polishing was varied with 5 etch depths from 0 to 15 µm (0 µm means no polishing). Half of the samples were diffused on both sides with $POCl_3$ after polishing.

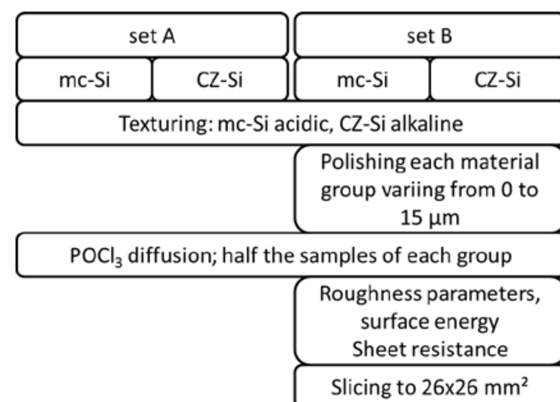

Figure 6: process flow and characterization of the prepared sample sets.

All samples of Set B have been characterized in different ways. The polishing removal was determined by weight of the samples. After all processes the sheet resistance was calculated with the data measured inductively before and after diffusion. The roughness parameters of every texture (0 µm polishing) and etched structures were measured with 3D laser measuring microscopy on one point of the sample. All samples got sliced into dices with 26x26 mm² size.

For each sample the surface energy is determined with a KRÜSS drop shape analysis 100 contact angle measurement device. Following the equation of YOUNG (eq. 1) the surface energy σ_s of solids can be calculated while measuring the contact angle θ. [6]

$$\sigma_s = \gamma_{sl} + \sigma_l * cos\theta \qquad \text{eq. 1}$$

σ_l is the known surface tension of the fluid and γ_{sl} is the surface tension between the solid and the liquid and needs to be determined as well.

With the FOWKES method, the surface tension between solid (s) and liquid (l) is separated into a polar (p) and dispersive (d) part as seen in eq. 2. [7]

$$\frac{\sigma_l(cos\theta+1)}{2} = \sqrt{\sigma_s^p}\sqrt{\sigma_l^p} + \sqrt{\sigma_s^d}\sqrt{\sigma_l^d} \quad \text{eq. 2}$$

The measurements for the surface energy were made with water as liquid with polar and dispersive part and diiodomethane as liquid without a polar part.

For both sample sets different etching solutions or fluids were used for the experiments. For set A water, HF-HNO_3 (32 g/l HF, 550 g/l HNO_3) optional with sulphuric acid or acetic acid as additives were used.

For set B non-silicon-etching aqueous solution in various concentrations (0 to 20 %) are used. The additives were acetic acid (HOAc), sulphuric acid (H_2SO_4), polyethylene glycol (PEG) and sodium dodecyl sulfate (SDS). These liquids are used in order to have different surface tensions. For all these fluids the surface tension were measured with a SITA science line t60 tensiometer in the auto mode. In this mode the surface tension is measured for varying bubble lifetime. [8]

3.2 Experimental setup

Each sample set was used for one experimental setup. Setup A (for sample set A) is a basin with one transparent window in a wall. In the basin are 4 pins holding a sample horizontally. In this basin a liquid can be filled and through the window the interaction between sample and liquid can be observed. For observing the experiment an Olympus i-Speed 2 high speed camera with 20 mm objective was used. As the meniscus is most interesting for the investigation the attention was mainly on the corner of the sample, seeing the edge in a planar view and in a side view (see figure 7)

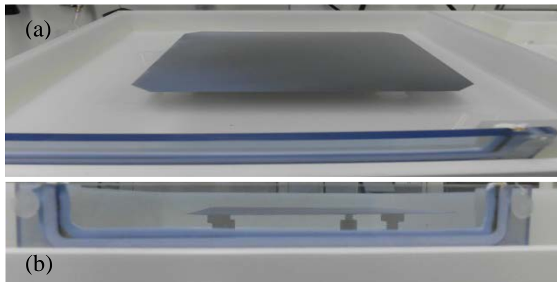

Figure 7: Top (a) and front (b) view of setup A

Setup B (for sample set B) is a vertical setup. The sample dice is fixed vertically in a dip coater holder. In a beaker the mentioned liquids are provided. With a velocity of 3mm/min the sample is immersed 8 mm into the liquid and held in this position for 60 s. After this static phase the sample is extracted with velocity of 3 mm/min. The dipping process is observed with two cameras. Both are AVT IEEE 1394a (Marlin) cameras. One has a 20 mm objective and captures the images at the edge of the sample. Thus the formed meniscus can be seen properly. The other camera has a 25 mm objective and shows the broad side of the sample. The meniscus cannot be observed properly but it is possible to differentiate the wetted and dry parts of the sample.

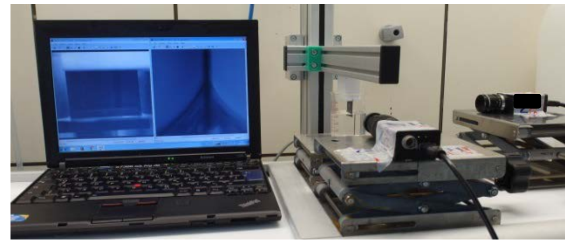

Figure 8: Setup B with two cameras, dip coater and beaker with sample and screen with the two camera views.

4 RESULTS AND DISCUSSION

4.1 Setup and Set A

For all samples combined with all liquids the interaction were observed including developing of the meniscus, reaction of the etching solutions with the sample and collapse of the meniscus. A strip of pictures taken for meniscus developing are shown in figure 9.

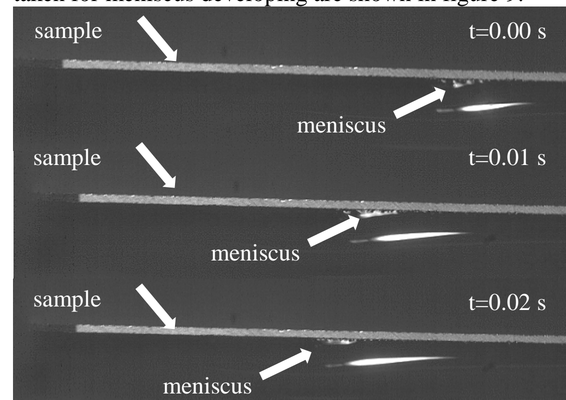

Figure 9: Developing of the meniscus for 0.02 s on an acidic textured mc-Si material without emitter and a HF-HNO_3-CH_3COOH etching solution.

Starting from the first contact point between fluid and solid the meniscus spreads and contacts the lower edge of the sample for all samples and liquids. For samples without emitter and thus assumed hydrophobic surface the meniscus stays as long at the lower edge as the etching reaction is not starting. For samples with hydrophilic surface (with emitter) the meniscus reacts different. For mc-Si the meniscus creeps to the higher edge if the solution contains CH_3COOH as additive. The same happens for CZ-Si if CH_3COOH or H_2SO_4 are added. In figure 10 this creeping is shown and highlighted with white lines. It was not observed if the liquid creeps around the edge onto the top of the sample.

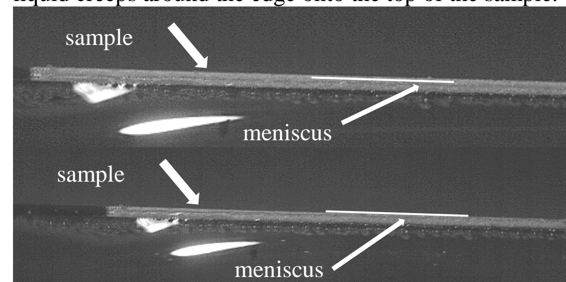

Figure 10: Creeping of the meniscus on the example of alkaline textured CZ-Si material with emitter and a HF-HNO_3-CH_3COOH etching solution.

The collapse of the meniscus was achieved by reducing the liquid volume from the basin. Thus, it was observed that for every sample and fluid the collapse appears the same. A kind of fluidic bridges is built between the liquid and sample before it ruptures while the liquid level falls further below. In figure 11 these bridges are shown.

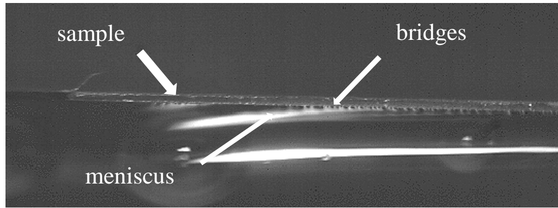

Figure 11: Collapsing meniscus and fluidic bridges on the example of alkaline textured CZ-Si material with emitter and a HF-HNO_3 etching solution.

The bridges appear probably as an effect of adhesion and cohesion of the etching solution and the sample surface.

As gas bubbles appear below the sample the chemical etching reaction has started already. Initially small bubbles increase in size and burst. If the edge is not wetted due to the creeping meniscus the bursting bubbles splash the etching fluid on the edge of the samples. Thus the meniscus can increase easily. Due to the chemical reaction this process repeats and the meniscus is rising continuously higher. In figure 12 a strip of pictures with a bursting bubble and a wetted sample edge can be seen.

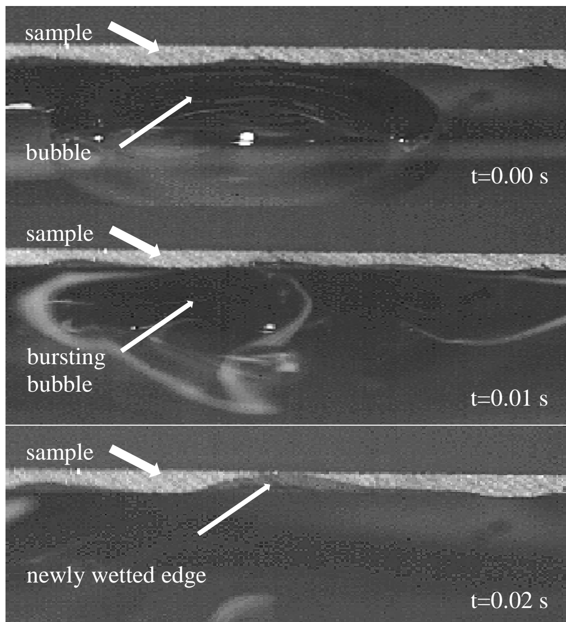

Figure 11: Bursting bubble during 0,02s on the example of acidic textured mc-Si material without emitter and a HF-HNO_3 etching solution.

If the sample edge is already wetted by creeping meniscus, bursting bubbles do not affect the edge anymore, but it was not observed whether the bursting bubbles wet the top side of the sample. It turns out, the smaller the bubbles smaller is the wetting of the sample edge. Additionally the bubble size depends on sample morphology, hydrophilic properties and etching solution. In the absence of an accurate scale the bubble sizes could not be measured but compared. Hydrophilic surfaces decrease the bubble size as well as acidic textures compared to alkaline textures. CH_3COOH as additive decreases bubble size as well. The HF-HNO_3 solution could not be compared with the HF-HNO_3-H_2SO_4 solution due to lack of proper pictures.

With all observations made in setup A, thesis a) and b) are rebutted. Anyway thesis a) was not absolutely wrong as bursting bubbles splash the sample edge and thus support the fluid wrap around. Concerning thesis b) a creeping meniscus only occurred within hydrophilic surfaces. Thus the hydrophilic properties have a major influence on the fluid wrap around. Furthermore for mc-Si and CZ-Si the creeping liquid are not the same. Thus the surface morphology seems to have an influence on the creeping as well.

Finally new theses arise out of the experiment with setup A:

a) Creeping of liquid and bursting bubbles cause fluid wrap around only
b) Creeping of liquid is depending on surface morphology, surface tension and hydrophilic properties of the surface
c) The effect of bursting bubbles on fluid wrap around is dependent of bubble size and status of sample edge
d) Bubble size is influenced by liquid, surface morphology and hydrophilic properties of the surface

4.1 Setup and Set B

Based on the results of setup A new experiments were planned. This setup investigates thesis b) of setup A.

In figure 12 the surface tension of acetic acid in relation to the number of readings is shown for all prepared concentrations.

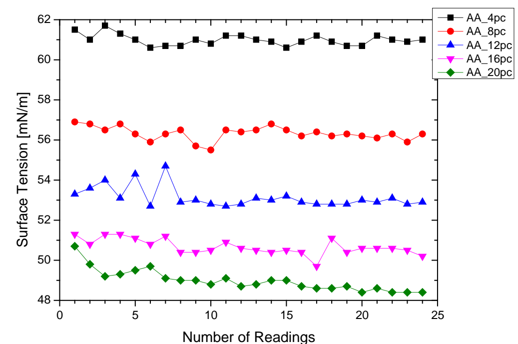

Figure 12: Surface tension of acetic acid in different concentrations (4-20 %] and repeated measurements

All measured and averaged surface tension data for all fluids and different concentrations are shown in table 1. For SDS, PEG and acetic acid the surface tension decreases but for sulphuric acid it is increasing with increasing concentrations. Acetic acid reaches the lowest surface tension and sulphuric acid the highest.

Table I: surface tension σ of used liquids in different concentrations

conc [%]	σ_{SDS} [mN/m]	σ_{PEG} [mN/m]	σ_{HOAc} [mN/m]	σ_{H2SO4} [mN/m]
0	72.35	72.35	72.35	72.35
0.5	70.83			
1	69.27			
1.5	68.21			
4	65.21	63.43	60.99	72.91
8	63.74	62.23	56.33	73.05
12	62.73	61.56	53.13	73.41
16	62.43	61.29	50.67	73.78
20	62.48	59.54	48.98	74.23

Assuming a dependency between surface tension and spreading, the highest meniscus is expected for acetic acid and the smallest for sulphuric acid.

In figure 13 an example of a measurement of the contact angle is shown. A drop is on the surface of the sample and for calculation of the contact angle a circle and a baseline is inserted. This measurement was made for all samples with diiodomethane and water several times and averaged.

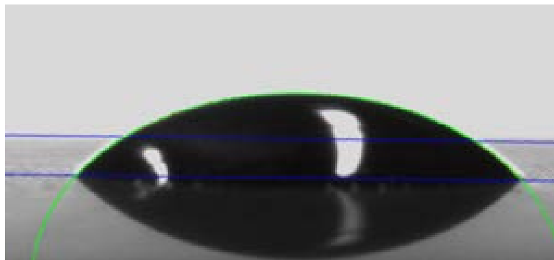

Figure 12: Diiodomethane drop on an alkaline textured CZ-Si surface. Baseline (blue) and circle (green) are inserted for contact angle calculation.

For samples with emitter or with polished surface the smallest surface energies are expected. These are calculated from the measured contact angles. The roughness is a more precise value for characterizing than polish depth. This is caused by varying initial textures and etching solutions resulting in different surface morphologies in spite of same polishing removal

In table 2 root mean square roughness S_q, disperse surface energy σ_d, polar surface energy σ_p and total surface energy σ_{total} are listed for the different materials Mat (mc, CZ), hydrophilic properties (T, E) and polishing depths (pol). The roughness of the samples is expected to decrease while surface energy is increasing with increasing etch removal. For intended 3 µm etch removal the polishing removal varied due to process inhomogenities from 0,5 to 1 µm from sample to sample. This is one more reason to use S_q for a more accurate comparison. For the textured CZ-Si samples with no polishing and 3 µm polishing the water drop spread immediately when contacting the surface due to a highly hydrophilic surface. Thus no contact angle could be measured and no surface energy was calculated. The mc-Si samples with emitter have higher surface energies than samples without emitter. The surface of the non-polished to 6 µm polished CZ-Si is more hydrophilic without emitter than with emitter. For both CZ-Si sample types the surface energy is decreasing with decreasing roughness. There are no explanations for this behavior yet.

Table II: root mean square roughness S_q, disperse surface energy σ_d, polar surface energy σ_p and total surface energy σ_{total} of used samples. mcT= mc-Si without emitter, mcE= mc-Si with emitter. CZT=CZ-Si without emitter, CZE= CZ-Si with emitter. Pol= polishing depth, Mat= material type.

Mat	pol µm	S_q µm	σ_d mN/m	σ_p mN/m	σ_{total} mN/m
mcT	0	0.65	22.37	32.50	54.86
mcT	3	0.72	26.76	24.16	50.91
mcT	6	0.60	24.53	36.87	61.40
mcT	10	0.27	25.20	35.27	60.77
mcT	15	0.24	28.10	31.66	59.77
mcE	0	0.66	24.80	37.44	62.23
mcE	3	0.76	26.00	40.12	66.13
mcE	6	0.39	28.59	35.49	64.08
mcE	10	0.49	24.58	39.90	64.48
mcE	15	0.36	22.90	40.81	63.71
CZT	0	0.91	-	-	-
CZT	3	0.84	-	-	-
CZT	6	0.56	26.83	36.64	63.47
CZT	10	0.42	28.39	26.98	55.38
CZT	15	0.34	23.86	35.05	58.90
CZE	0	0.83	22.31	44.94	67.25
CZE	3	0.82	26.74	40.55	67.29
CZE	6	0.68	22.89	38.73	61.62
CZE	10	0.48	23.70	42.59	66.29
CZE	15	0.40	20.27	42.17	62.44

In figure 13 examples of a front view and side view image of setup B are shown. Additional lines for measuring the meniscus angle φ, the front view height h_{fv} and the side view height h_{sv} are inserted. These heights are measured from the liquid base line. On the side view a creeping of the liquids at the sample edge could be observed for all samples. This creeping happens on one side only and is caused by the laser damage arising by slicing the samples. On the other side this creeping does not occur. Thus the side view height is measured in the middle of the sample. The meniscus angle is measured for all samples in the same way by inserting parallels with distance of 100 µm and applying the angle legs on the sample surface and on the intercept point of the line with the meniscus. For smaller meniscus angles higher meniscus heights are expected.

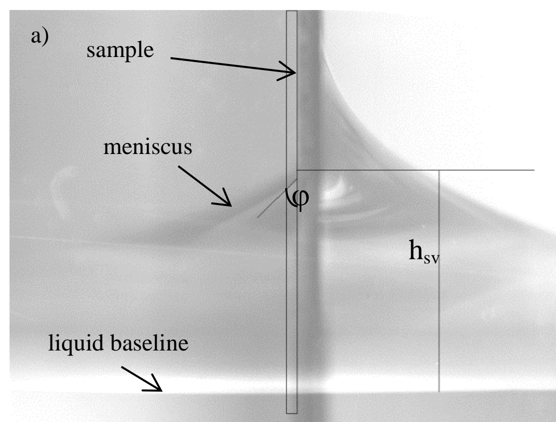

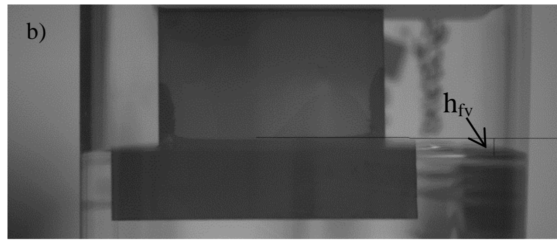

Figure 13: a) side view of mc-Si in 20% acidic acid with meniscus angle and side height. b) front view with front height

According to the results of surface energy with or without emitter and the surface tension of the liquids with changing concentration, expectations of the behavior of the meniscus can be made. These are an increasing meniscus height for mc-Si samples with emitter compared to mc-Si without emitter and opposite for CZ-Si. This expectation is based on the surface energy of the non-polished samples with and without emitter. Another expected effect based on surface tension is a decreasing meniscus height for higher sulphuric acid concentrations and opposite for all other additives. In general a higher meniscus height is expected for CZ-Si due to higher surface energy and for high acetic acid concentration due to low surface tension.

Not all samples and liquids have been measured yet. Already received values are shown in table 3.

Table III: meniscus angle φ, the front view height h_{fv} and the side view height h_{sv} of used samples. mcT= mc-Si without emitter, mcE= mc-Si with emitter. CZT=CZ-Si without emitter, CZE= CZ-Si with emitter. H_2SO_4=sulphuric acid, HOAc=acetic acid, Mat= material type, conc=concentration of liquid.

Mat	liquid	conc [%]	φ	h_{sv} [mm]	h_{fv} [mm]
mcT	H_2SO_4	4	39.4	3.0	1.7
mcT	H_2SO_4	20	61.2	1.9	2.7
mcE	H_2SO_4	4	37.2	3.1	2.9
mcE	H_2SO_4	20	40.0	2.7	2.1
CZT	H_2SO_4	4	37.6	-	17.9
CZT	H_2SO_4	20	41.9	3.1	18.3
CZE	H_2SO_4	4	30.0	2.8	-
CZE	H_2SO_4	20	33.0	2.7	3.9
mcT	HOAc	4	34.0	2.6	1.9
mcT	HOAc	20	45.4	1.9	2.3
mcE	HOAc	4	37.7	3.0	2.8
mcE	HOAc	20	33.1	2.7	2.3
CZT	HOAc	4	35.5	-	17.9
CZT	HOAc	20	36.6	3.0	18.7
CZE	HOAc	4	27.4	2.8	-
CZE	HOAc	20	34.8	2.7	3.9
mcT	PEG	4	47.5	2.2	2.4
mcT	PEG	20	48.1	2.0	2.1
mcE	PEG	4	32.6	3.1	2.9
mcE	PEG	20	35.4	2.6	2.4
CZT	PEG	4	35.7	-	18.0
CZT	PEG	20	31.6	3.0	18.0
CZE	PEG	4	33.0	2.8	-
CZE	PEG	20	31.2	2.7	4.1
mcT	SDS	0.5	-	-	1.9
mcT	SDS	20	51.34	1.7	2.2
mcE	SDS	0.5	35.4	3.1	3.1
mcE	SDS	20	34.8	2.7	2.6
CZT	SDS	0.5	34.3	3.1	17.6
CZT	SDS	20	34.4	3.1	18.7
CZE	SDS	0.5	29.8	2.8	-
CZE	SDS	20	34.3	2.8	4.0
mcT	H_20	nil	52.1	2.1	2.6
mcE	H_20	nil	20.8	2.3	2.3
CZT	H_20	nil	29.7	2.0	-
CZE	H_20	nil	28.9	2.5	4.1

Only non-polished samples are measured with the lowest and highest liquid concentrations yet. Thus correlations considering the changing of surface energy by polishing cannot be made. Due to some non-measurable contact angles and heights data is missing.

As can be seen in table 3 not all expectations concerning the meniscus height occur in the experiment. Increased meniscus heights are investigated due to surface energy, but the expected effects due to surface tension can only be seen for sulphuric acid. Another factor seems to influence the meniscus height besides the surface tension. This can be seen as well, as the meniscus heights for the different additives are not varying that much despite different surface tensions. The expected correlation between meniscus height and angle cannot be seen.

Up to now no part of thesis b) made out of setup A could be disproved, but it is proven, that surface tension is only one part of the liquids properties influencing the creeping. More measurements are needed to find clearly dependencies between surface tension, surface energy and surface morphology.

5 CONCLUSIONS

Since no clear correlations could be found from the previous measurements and no more theses could be proven, more measurements are necessary. All mentioned samples and liquids of setup B will be measured in further experiments as well as viscosity of the liquids. Assuming to find clear correlations for thesis b) further investigations will be made concerning thesis c) and d). A horizontal setup will be used as well as etching solutions as in setup A. In this experiment the bubbles shall be investigated in dependence of all already mentioned factors. The bubble size and lifetime and again meniscus behavior will be measured. Meaning to completely avoid the fluid wrap around, even more experiments are planned in an industrial single side etching tool including the influences of dynamic fluid flow and wafer transportation.

REFERENCES

[1] Blakers, A.W., et al., 22.8% efficient silicon solar cell. Applied Physics Letters, 1989. 55(13): p. 1363
[2] Kranz, C., et al., Impact on the rear surface roughness on industrial-type PERC solar cells, Proceedings of the 27th European Photovoltaic Solar Energy Conference and Exhibition, 2012
[3] Cornagliotti, E., et al., How much rear side polishing is required? A study on the impact of rear side polishing in PERC solar cells., Proceedings of the 27th European Photovoltaic Solar Energy Conference and Exhibition, 2012, 561-566
[4] Rentsch, J., Ackermann, R., Challenges for single-side chemical processing, Photovoltaics International 16: 7, 2012
[5] Richter, M. et al., A novel approach for single side wet chemical polishing of crystalline silicon solar

cells, Proceedings of the 28th European Photovoltaic Solar Energy Conference and Exhibition, 2013
[6] T. Young; Phil.Trans.Roy.Soc. London 95 (1805), 65
[7] F. M. Fowkes, Attractive Forces at Interfaces. In: Industrial and Engineering Chemistry 56, 12 (1964), P. 40-52.
[8] V. B. Fainerman and R. Miller, "Maximum bubble pressure tensiometry - an analysis of experimental constraints", Advances in colloid and interface science 108-109 (2004) 287.